Bulletin of the Seismological Society of America, Vol. 92, No. 6, pp. 2333–2351, August 2002

Mapping the Sources of the Seismic Wave Field at Kilauea Volcano, Hawaii, Using Data Recorded on Multiple Seismic Antennas

by Javier Almendros, Bernard Chouet, Phillip Dawson, and Christian Huber

Abstract Seismic antennas constitute a powerful tool for the analysis of complex wave fields. Well-designed antennas can identify and separate components of a complex wave field based on their distinct propagation properties. The combination of several antennas provides the basis for a more complete understanding of volcanic wave fields, including an estimate of the location of each individual wave-field component identified simultaneously by at least two antennas. We used frequency–slowness analyses of data from three antennas to identify and locate the different components contributing to the wave fields recorded at Kilauea volcano, Hawaii, in February 1997. The wave-field components identified are (1) a sustained background volcanic tremor in the form of body waves generated in a shallow hydrothermal system located below the northeastern edge of the Halemaumau pit crater; (2) surface waves generated along the path between this hydrothermal source and the antennas; (3) back-scattered surface wave energy from a shallow reflector located near the southeastern rim of Kilauea caldera; (4) evidence for diffracted wave components originating at the southeastern edge of Halemaumau; and (5) body waves reflecting the activation of a deeper tremor source between 02 hr 00 min and 16 hr 00 min Hawaii Standard Time on 11 February.

Introduction

The ground motion recorded at a seismic station represents the contributions from a variety of sources of natural and artificial origins. When a single source dominates the wave field within a particular frequency range, its analysis can be relatively straightforward. This is the case in earthquake seismology, where seismograms are interpreted as a succession of seismic phases clearly detected above a background noise that includes any other component of the wave field. However, when two or more coherent phases arrive simultaneously, the ground motion recorded at a single station is not sufficient to separate them. In this case, different tools are required for separation and identification of the wave-field components, capable of providing a spatial as well as a temporal sampling of the wave field within a region. These tools are seismic antennas.

Seismic antennas have been widely used to analyze complex wavefields. Two approaches have mainly been used in these analyses. The first approach consists of the application of the spatial correlation method (Aki, 1957). This method assumes that the wavefield is stochastic and stationary in time and space, and it calculates average autocorrelation coefficients to characterize the wave types present in the wave field. The method yields estimates of the dispersion characteristics of the surface-wave components of the wave field, which can be used to explore the shallow velocity structure beneath the array (Ferrazzini *et al.*, 1991; Métaxian *et al.*, 1997; Chouet *et al.*, 1998). The second approach applies the concepts of velocity filtering and beamforming. This procedure consists of an estimation of the level of coherence between array traces as a function of the apparent slowness vector, whose components (apparent slowness and propagation azimuth) define the propagation properties of the wave fronts. Examples of such procedures are the array-averaged cross-correlation (Del Pezzo *et al.*, 1997; Almendros *et al.*, 1999), the frequency–slowness power spectrum estimated by beamforming (LaCoss *et al.*, 1969), the high-resolution wave-number spectrum (Capon, 1969), or the MUSIC algorithm (Schmidt, 1986; Goldstein and Archuleta, 1987). The occurrence of peaks above a noise threshold for certain values of the apparent slowness vector identifies the apparent slownesses and propagation azimuths of coherent components of the wave fields. An application of these methods thus allows an identification of the coherent signals present in the wave field and an estimation of their apparent slownesses and propagation azimuths. This approach is usually referred to as "wave-field decomposition." Most attempts at wave-field decomposition using single antennas have focused on the dominant component of the wave field (Goldstein and Chouet, 1994; Chouet *et al.*, 1997; Almendros *et al.*, 1999; Ibáñez *et al.*, 2000), although a few have

also analyzed the remaining coherent components (Gupta *et al.*, 1990; Del Pezzo *et al.*, 1997; Saccorotti *et al.*, 2001).

The use of multiple antennas is advantageous for several reasons. The most obvious is that they can provide joint location of the source of recorded seismicity based on independent estimates of the apparent slowness vectors obtained at each antenna. This is useful to locate events for which it is not easy to determine phase-arrival times. For example, this is the case of noisy earthquake records (Almendros *et al.*, 2000) or long-period (LP) seismicity in the field of volcano seismology (Almendros *et al.*, 2001a,b). For successful application of the joint location method, the temporal windows of data selected to estimate the slowness vectors must include the same wave fronts. In favorable situations, this can be ensured by comparing the waveforms recorded at different antennas. However, when the signal-to-noise ratio is small or when dealing with sustained wave trains, this basic requirement might be difficult to satisfy.

In this article, we combine the ideas of wave-field decomposition and joint location using multiple antennas to locate the sources of distinct coherent waves contributing to the wave field. We use frequency–slowness analyses of seismic-array data recorded on three synchronized antennas to identify wave-field components and determine their propagation properties and use the results from each antenna to perform joint locations and map the sources generating the recorded wave field.

Experiment and Data

A seismic experiment aimed at the identification of seismic sources within Kilauea volcano, Hawaii, was carried out by a joint Japan–United States team during the first weeks of February, 1997. The deployed instrumentation includes three small-aperture seismic antennas named D, E, and F (Fig. 1), featuring Mark Products L11-4A and L22-3D short-period sensors, each with a natural frequency of 2 Hz. Separate data loggers were used for each seismometer. All instruments used a common Global Positioning System (GPS) time base with an accuracy of 5 μsec among all channels. Antenna D has an aperture of 400 m and consists of 41 three-component sensors deployed in a semicircular spoked pattern, with a station spacing of 50 m along the spokes and an angular spacing of 20° between spokes. Antenna E, with an aperture of 300 m, also has a semicircular spoked configuration and includes 22 vertical-component sensors with a station spacing of 50 m along the spokes and an angular spacing of 30° between spokes. Antenna F has an aperture of 700 m and consists of 12 vertical-component sensors set up in a rectangular pattern with a station spacing of 200 m.

The seismic activity recorded during February 1997 was dominated by shallow LP seismicity (Chouet, 1996) in the form of a dense swarm of LP events superimposed on a background of sustained low-amplitude volcanic tremor. The peak in swarm activity occurred on February 11 and 12, reaching almost 100 LP events detected per hour. LP events recorded at Kilauea are characterized by a spindle-shaped amplitude envelope and a spectrum that contains energy in the band 1–15 Hz, with dominant peaks in the 2–6-Hz range. Individual-event durations are typically ~20 sec. Low-amplitude tremor bursts, which persist for a few tens of seconds when no LP events are present, show spectral characteristics similar to those of LP events.

Several analyses have already been performed on these data. Saccorotti *et al.* (2001) studied the wavefield properties of an LP event and tremor sample, and described some of the characteristics that are common to all LP seismicity from this region. Almendros *et al.* (2001b) located the sources of 1129 LP events and 147 samples of tremor by using the joint location method developed by Almendros *et al.* (2001a). Their results demonstrate that the source of LP activity recorded during the 1997 experiment originates in a shallow hydrothermal system located northeast of the Halemaumau pit crater. Finally, Almendros *et al.* (2002) analyzed a sample of traffic noise to explore the capabilities of the antennas to track a moving source.

Frequency–Slowness Analyses

The propagation properties of a seismic signal at the free surface are specified, under a plane wave-front approximation, by the apparent slowness vector **s**. The magnitude of this vector, the apparent slowness, **s**, represents the inverse of the apparent velocity of the wave fronts as they propagate horizontally across the surface. The vector direction, measured clockwise from north, represents the wave propagation

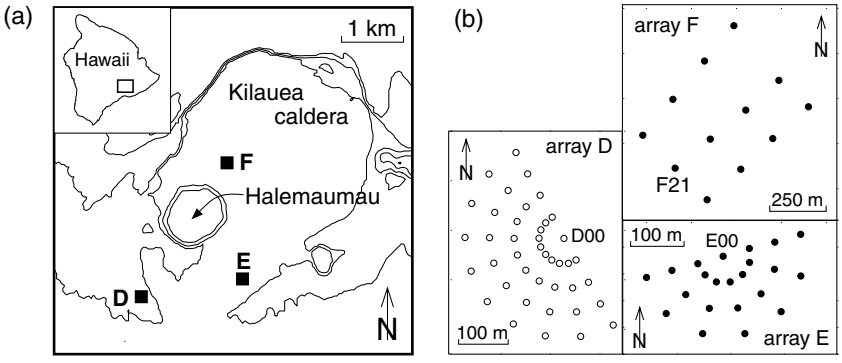

Figure 1. (a) Map of the Kilauea caldera, showing the positions of the centers of seismic antennas D, E, and F (black squares). The inset box shows the position of the area of study on the island of Hawaii. (b) Configuration of the seismic antennas. Open circles are three-component instruments, and black dots represent vertical-component sensors. D00, E00, and F21 are receivers from which the sample seismograms in Figs 3–8 are extracted.

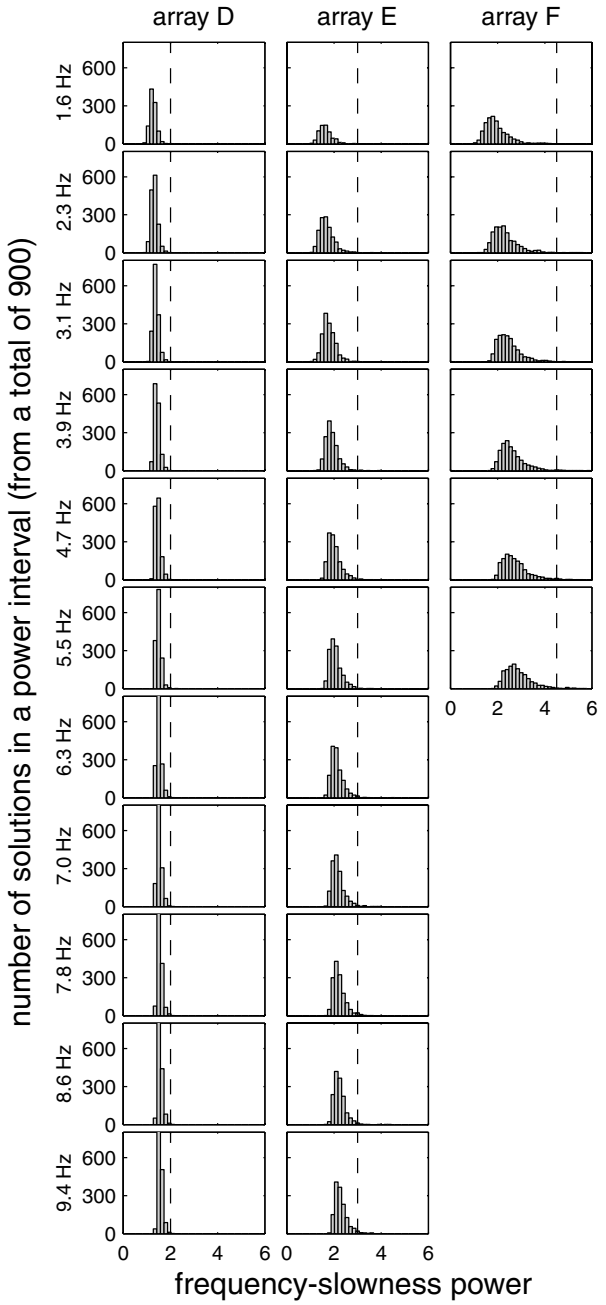

Figure 2. Histograms of frequency–slowness power obtained in different frequency bands for random noise samples at arrays D, E, and F. The dashed lines mark the cutoff values selected to restrict the analysis to coherent solutions.

azimuth ϕ. Several methods are available to extract information on the slowness vectors of a wave field from array data. The most useful approach for the purpose of understanding the wave-field composition consists of an estimation of the frequency–slowness spectrum based on the multiple signal classification (MUSIC) algorithm (Schmidt, 1986; Goldstein and Archuleta, 1987). This method has the advantage of providing better resolution capabilities for secondary sources than most other methods.

Frequency–slowness analyses of vertical-component data from antennas D and E were performed in 11 overlapping frequency bands with an individual bandwidth of 1.2 Hz covering the band 1–10 Hz. The slowness domain spanned a range of slownesses up to 2 sec/km with a sampling interval of 0.1 sec/km. Because of the relatively sparse receiver configuration of antenna F, data from this antenna were analyzed over narrower ranges of frequencies and slownesses. Array F data were analyzed in six overlapping frequency bands with an individual bandwidth of 1.2 Hz covering the band 1–6 Hz, and slownesses were limited to values ranging up to 1 sec/km using a tighter slowness sampling interval of 0.05 sec/km. Frequency–slowness estimates were obtained in a 2.56-sec-long window (256 samples) sliding in increments of 0.2 sec across the records. Estimates of the slowness vectors of the two main components of the wave field were obtained in each window.

The dominant peak in the slowness spectrum for a given frequency band represents the most coherent component of the wave field, whereas the secondary peak, if present, represents a secondary component of the wave field with lower coherence across the array. Other peaks may also be present in complex wave fields, but we make no attempt here to resolve more than two spectral peaks in our data. This does not mean that our procedure focuses exclusively on two particular components of the wave field. In fact, analyses of the two peaks, done over a period of time, reveal a variety of wave-field components because different components become dominant at different times in the records. As a result of this procedure, we obtain estimates of the apparent slownesses and propagation azimuths of the two main components of the wave field at each antenna and for each frequency band in the form of time series.

We performed frequency–slowness analyses for >26 hours of array data, including two time intervals that sampled the most active period of the LP swarm (from 19 hr 00 min on 11 February to 03 hr 00 min on 12 February and from 13 hr 00 min on 12 February to 00 hr 00 min on 13 February) and four individual 1-hour periods that sampled activity during the preceding few days (21 hr 00 min–22 hr 00 min on 8 February, 01 hr 00 min–02 hr 00 min on 9 February, 16 hr 00 min–17 hr 00 min on 10 February, and 01 hr 00 min–02 hr 00 min on 11 February). Antenna F was not in operation during the period from 16 hr 00 min to 19 hr 00 min on 11 February; therefore, this period is analyzed with data from antennas D and E only. All times used throughout the present article are Hawaiian Standard Time.

To minimize contributions from noise and ensure a minimum level of coherence, only solutions with a frequency–slowness power above a certain threshold are considered. The determination of this threshold is based on array analyses of random noise. We generate 180-sec-long synthetic seismograms containing white noise and filter these synthetics in the 1–15 Hz band to simulate the frequency content of the actual records. Frequency–slowness analyses are then performed on the synthetics by following the same proce-

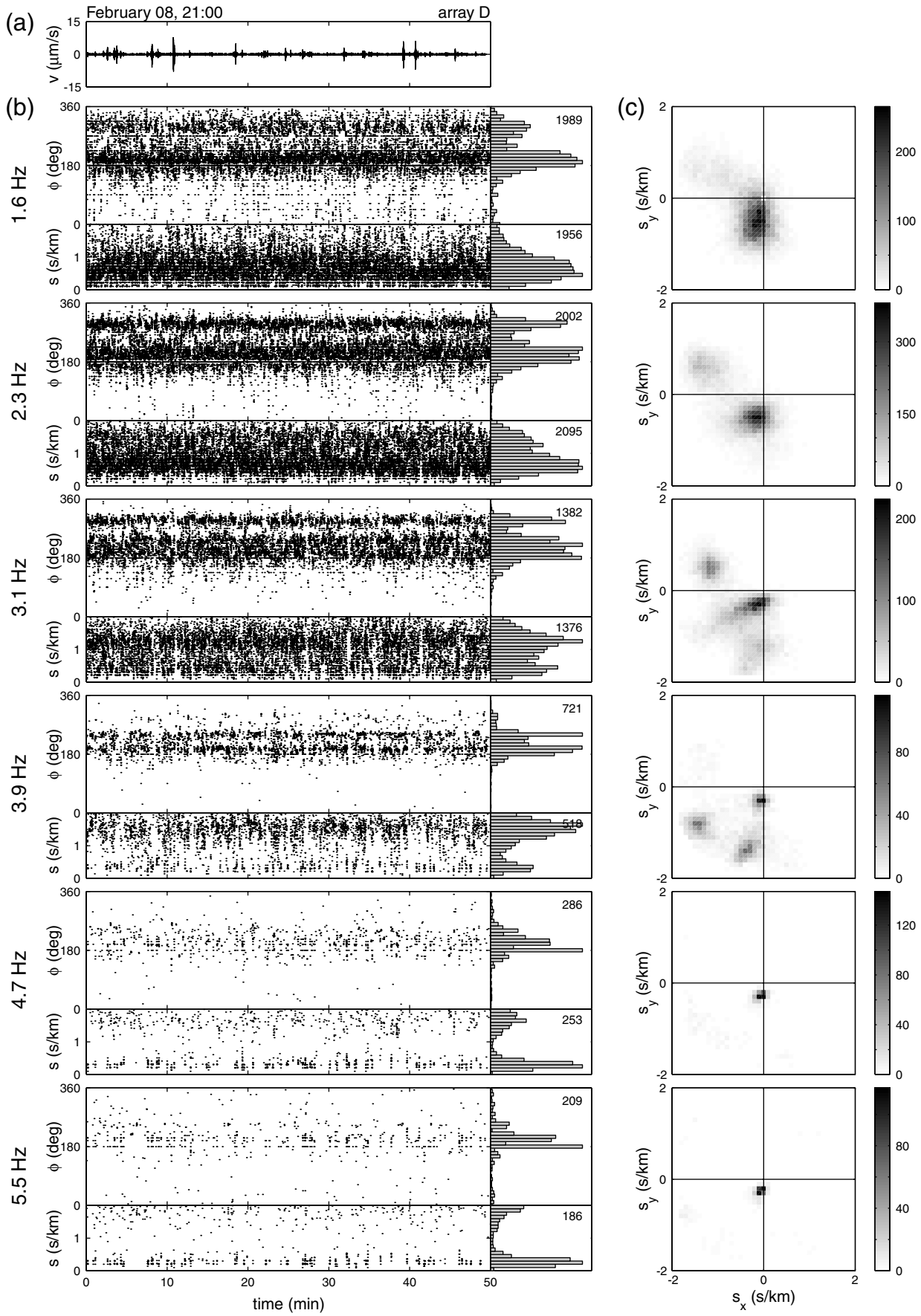

Figure 3. (*Caption on facing page*)

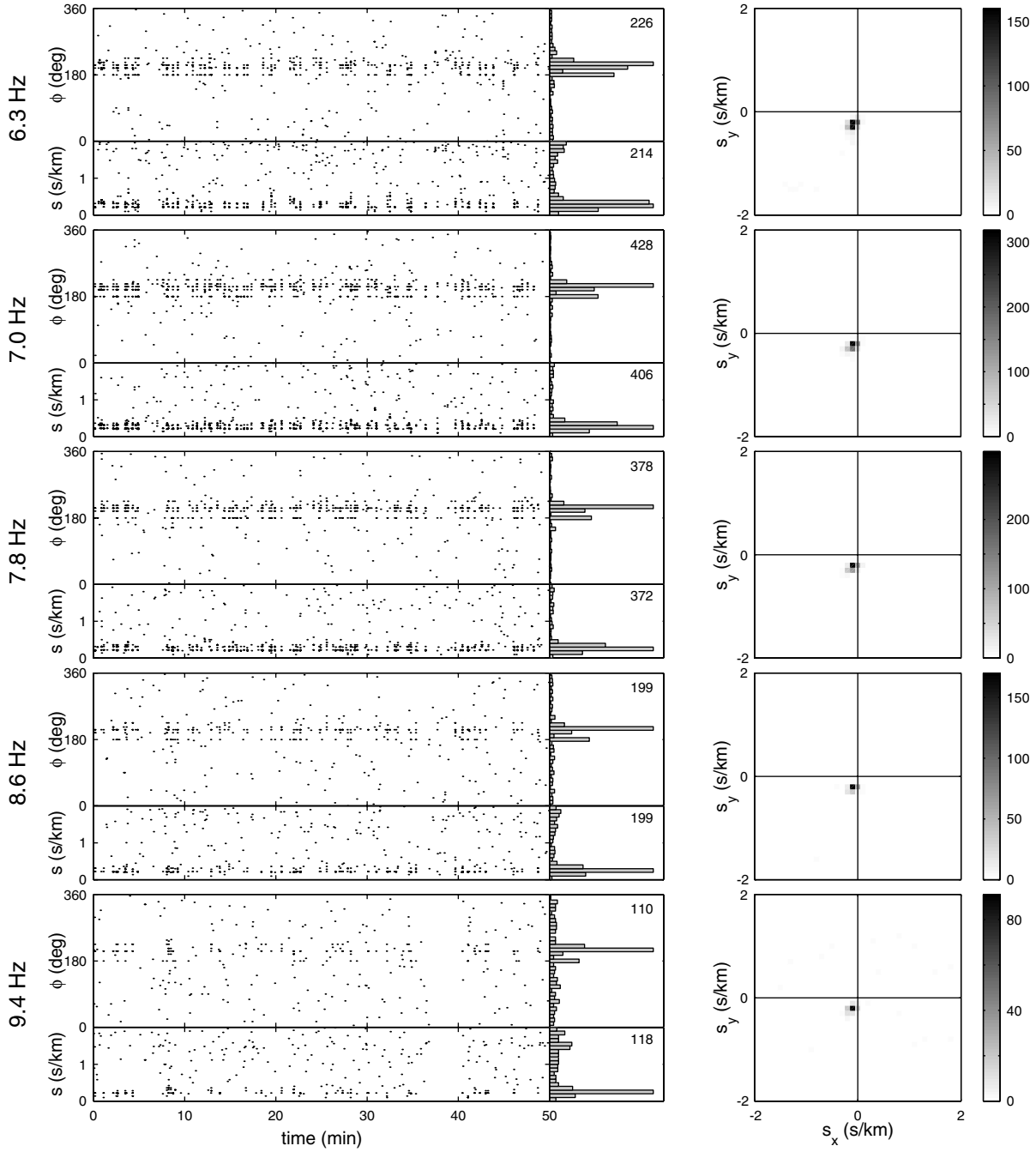

Figure 3. (a) Sample seismogram at station D00 (see Fig. 1), showing 50 minutes of data starting at 21 hr 00 min on 8 February. (b) Estimates of azimuths and apparent slownesses obtained in different frequency bands from frequency–slowness analyses of data from array D. At the right of each time series are histograms showing the distributions of azimuths and slownesses. The number of solutions contained in the most populated histogram bin is shown in the upper right corner of the panel. (c) Two-dimensional histograms in the slowness domain obtained for each frequency band. The peaks in these histograms identify the most common slowness vectors resolved in the frequency–slowness data during the interval shown in (a).

dure as described previously for real data. Figure 2 shows histograms of frequency–slowness power obtained from these analyses. Power estimates differ at each antenna, mainly because of the different array configurations. The selected cutoff values are 2, 3, and 4.5 for antennas D, E, and F, respectively. Note that the magnitude estimated by the MUSIC method is a nondimensional number, even though this number is usually referred to as the frequency–slowness power spectrum (Goldstein and Chouet, 1994; Chouet *et al.*, 1997; Saccorotti *et al.*, 2001; Almendros *et al.*, 2001a). The use of such appelation is justified by the similarity between the physical interpretation of MUSIC re-

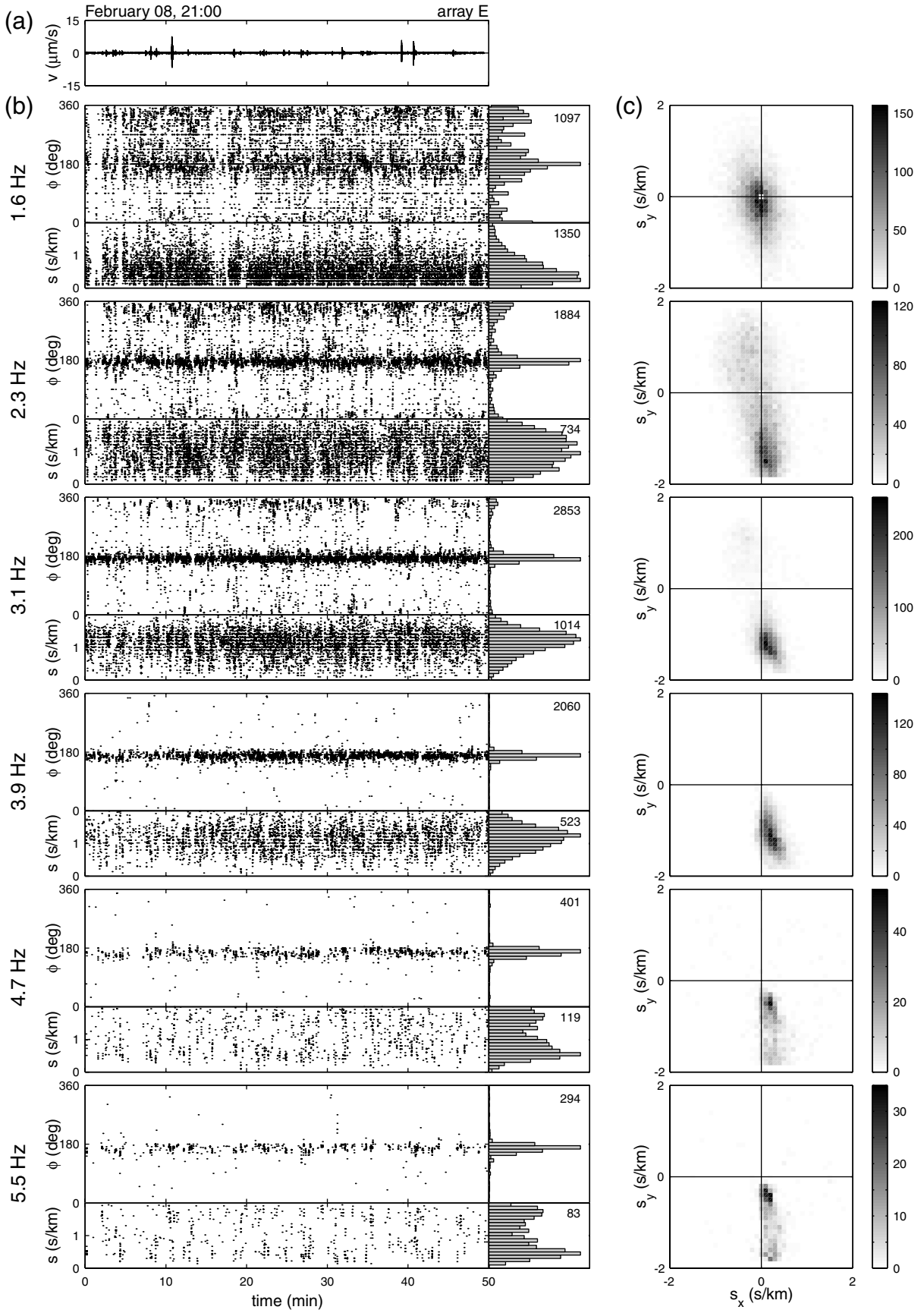

Figure 4. Same as Fig. 3, for antenna E.

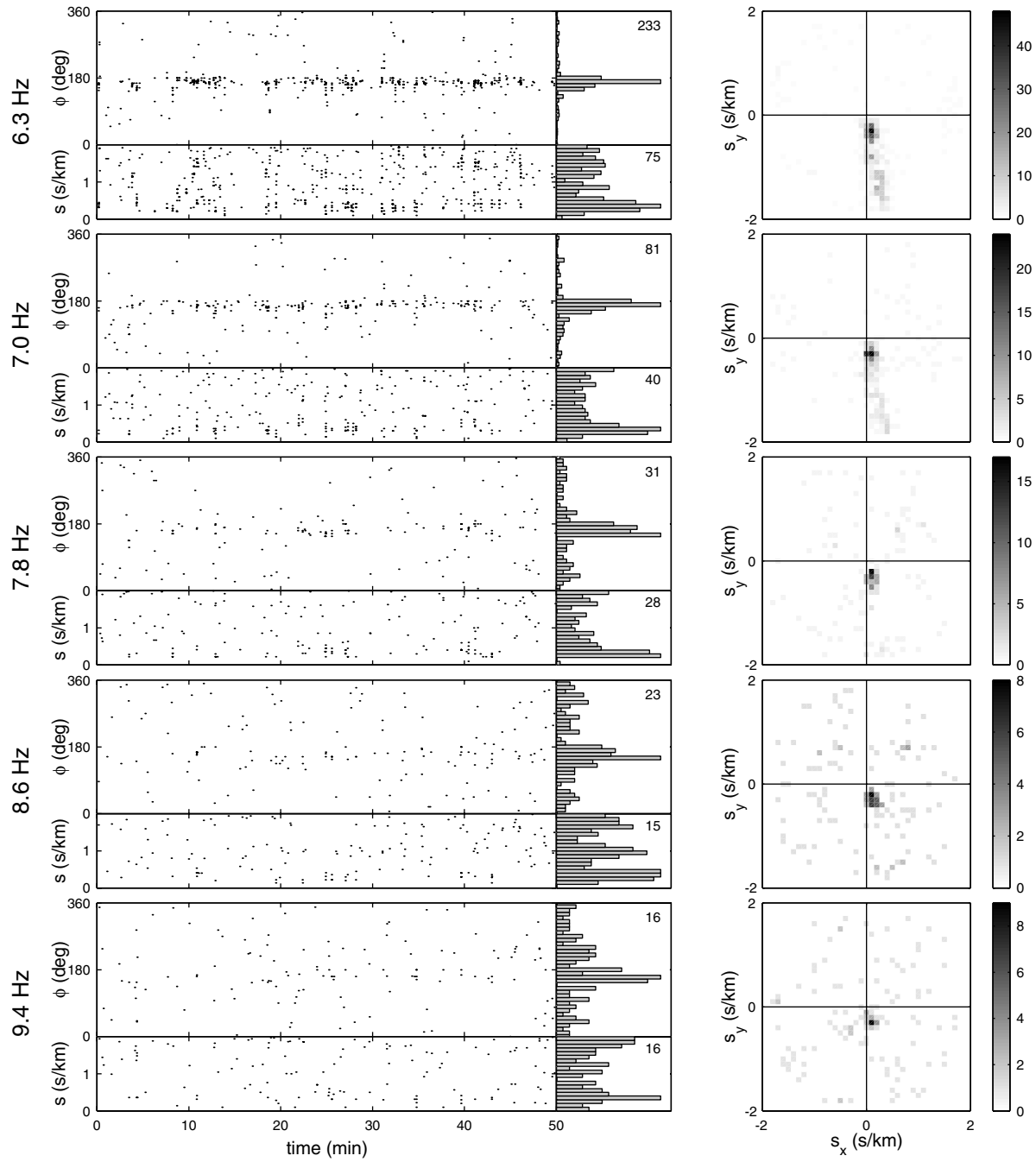

Figure 4. Continued.

sults and estimates of the actual frequency–slowness power spectrum of array data (Capon, 1969; LaCoss *et al.*, 1969).

Figures 3–5 are examples of frequency–slowness results obtained in different frequency bands at each antenna. The most striking feature of these results is found in the azimuthal plots, which show a clustering of solutions around particular directions. These directions remain stationary not only during the interval shown in the figures but also during the entire interval lasting >4 days considered in our study. At each antenna, one of the directions is frequency independent; that is, the same cluster of azimuths is observed in almost all of the frequency bands considered, although the clusters tend to disappear in the high-frequency bands because of a lack of resolution. Other secondary directions are also observed at arrays D and E, but these are well defined only within a limited frequency range. The distributions of apparent slownesses are generally broad in the low-frequency bands, pointing to the presence of both body and surface waves in the wave field. There are also clusters around specific slowness values, although this clustering is not as clear as in the azimuth data. The most apparent cluster corresponds to slownesses between 0.3 and 0.5 sec/km, and

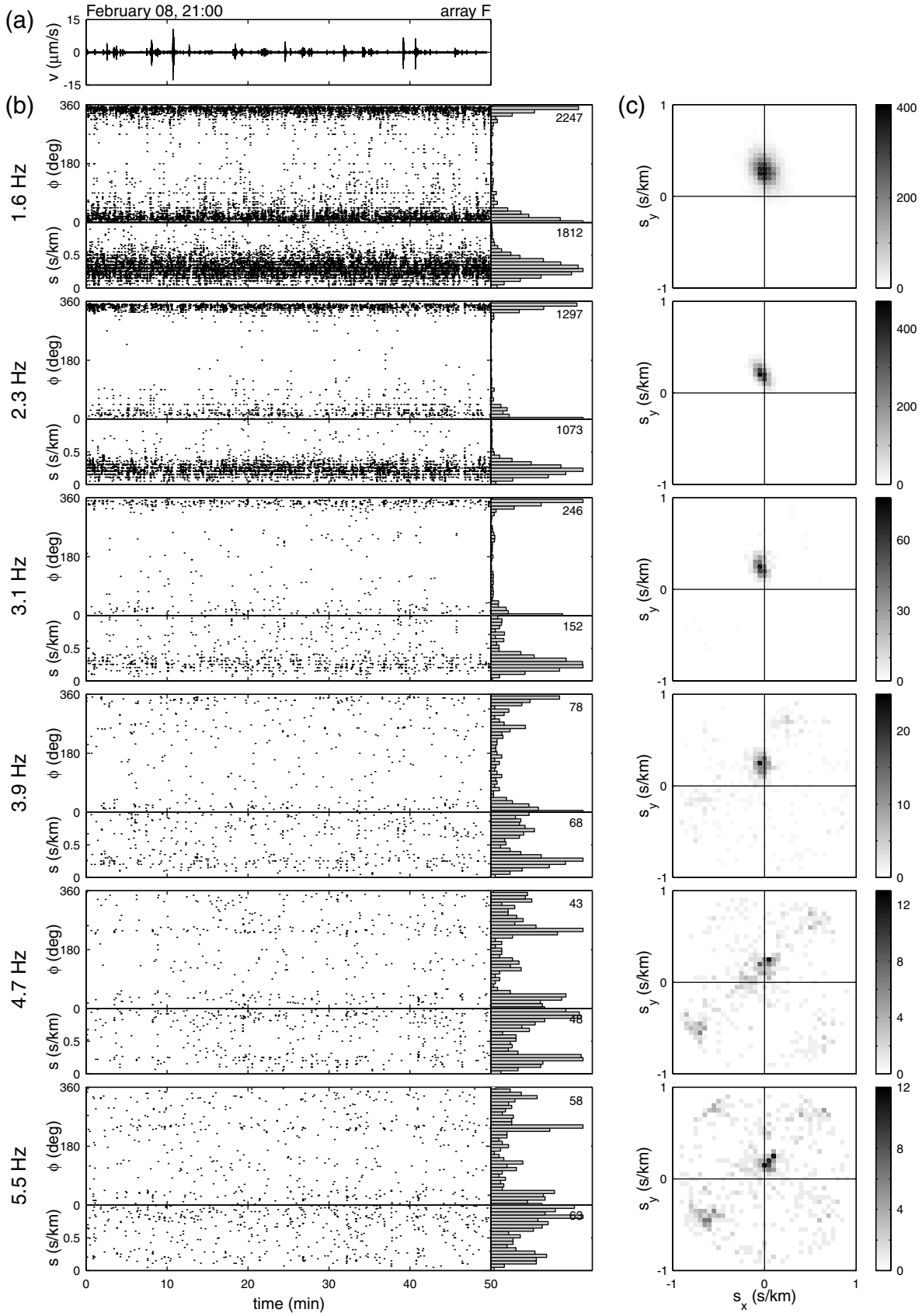

Figure 5. Same as Fig. 3, for antenna F.

is best defined at arrays D and F. This cluster corresponds to the main cluster of azimuths observed at each antenna, as is readily apparent in the two-dimensional histograms.

Most of the features described in this article remain stationary during the entire time interval analyzed, except for a change noted on 11 February. This change occurs relatively suddenly, between 02 hr 00 min and 16 hr 00 min on that day, unfortunately during a period when the antennas were not in operation. Figures 6–8 show the frequency–slowness results obtained in the different frequency bands at each antenna for 50 minutes of data starting at 19 hr 00 min on 11 February. The main distinction from the previous data shown in Figs. 3–5 is in the apparent slownesses, which are found to be smaller in the low-frequency bands. This results in a greater scattering of azimuths, which makes it difficult to recognize any clusters at all, although the preferred directions are still present in the data, as shown in the histograms. We will refer to the two different behaviors observed before and after the morning of 11 February as period 1 and 2, respectively.

Table 1 lists the azimuths and apparent slownesses of the most common slowness vectors observed during the 4-day interval analyzed, together with the frequency bands and periods during which these vectors are seen, and a number used to identify them. The individual vectors are plotted in Fig. 9 to help visualize the propagation characteristics of the different wave-field components.

Wave-Field Decomposition and Source Location

The frequency–slowness analyses provide a decomposition of the wave fields recorded at Kilauea in terms of propagation properties. The results show evidence of at least three different wave-field components with distinct propagation parameters. The purpose of this section is to identify each of these components, estimate the position of the source, and suggest plausible processes by which these components might have been generated at Kilauea volcano during the time period considered.

Although not included in the present study, traffic noise generated along a road crossing Kilauea caldera is yet another component contributing to the wave field observed in our analyses. This component is detected as several-minutes-long bursts of energy propagating with very large slownesses and slowly varying azimuths, occurring mostly during the central hours of the day. A more detailed analysis of the traffic noise was performed in a separate study (Almendros *et al.*, 2002).

Hydrothermal Source Component

The dominant wave-field component identified by all antennas is represented by peaks D1, E1, and F1 (see Table 1 and Fig. 9). This component has the following characteristics: (1) it propagates with azimuths of 210°, 170°, and 355° across arrays D, E, and F, respectively, indicating that its source is located somewhere near the eastern edge of the Halemaumau pit crater; (2) its apparent slownesses are relatively small, on the order of 0.2–0.5 sec/km, pointing to apparent velocities in the range 2–5 km/sec, consistent with body waves; (3) it contains coherent energy within a broad frequency band, ranging from 1 up to 10 Hz (up to 4 Hz at antenna F); and (4) it is always present in the wave field during the period analyzed. These directional properties are especially clear at higher frequencies, even though the total number of solutions is smaller, because this component is the only one that remains coherent at high frequencies.

To understand the origin of this dominant component of the wave field, we compare its propagation properties to those obtained by Almendros *et al.* (2001b) in frequency–slowness analyses of LP events and tremor extracted from the same data set as that investigated in the present article. Almendros *et al.* (2001b) found that the propagation azimuths and slownesses of LP events and tremor samples were more or less constant at each antenna (Fig. 10). These propagation parameters are similar to those described above for peaks D1, E1, and F1. Such coincidence suggests that the LP seismicity and dominant component of the wave field share a common source. This source not only produces discrete LP events and tremor bursts but also remains active during the entire time interval analyzed. Therefore, we identify the dominant component of the wave field as background volcanic tremor. The source region identified by Almendros *et al.* (2001b) is contained within a volume of 0.09 km^3 located at depths shallower than 500 m near the northeastern edge of Halemaumau (Fig. 11). As in Almendros *et al.* (2001b), we identify this region as a hydrothermal system whose activity produces the detected tremor.

Scattered Waves

Secondary components of the wave field are represented by slowness vectors D2, D3, D4, E2, and E3 (see Table 1 and Fig 9). These components have the following characteristics: (1) they propagate with azimuths of 210°, 240°, and 300° at array D, and 170° and 330° at array E; (2) their apparent slownesses are larger than 1 sec/km, suggesting the presence of a shallow source generating surface waves; (3) these waves are clearly detected by the dense receiver configurations in antennas D and E, but their large apparent slownesses preclude their detection by the sparse receiver distribution in antenna F; (4) the coherence of these components is limited to a few frequency bands (see Table 1); and (5) although these waves are always present in the wave field, they are most clearly detected during the first part of the LP swarm (period 1).

The waves identified by peaks D2 and E2 have the same directions as the waves identified by peaks D1 and E1 and thus must originate in the same source region. Our interpretation is that D2 and E2 represent surface waves generated along the path between the LP source and antennas D and E.

The situation is different with peaks D4 and E3. These waves are also generated by shallow sources; however, they originate in an area where there is no reported volcanic

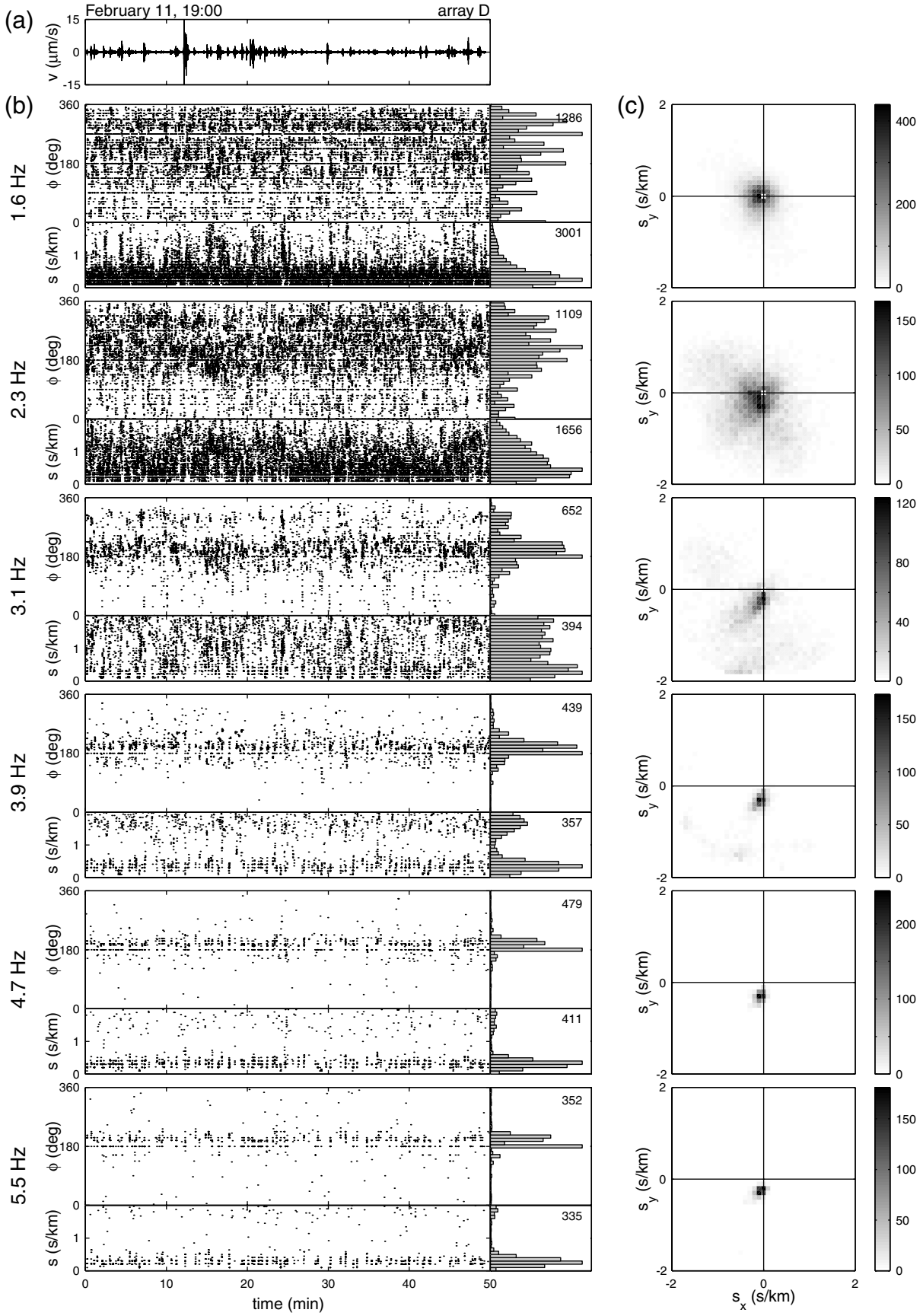

Figure 6. Same as Fig. 3, for data starting at 19 hr 00 min on 11 February.

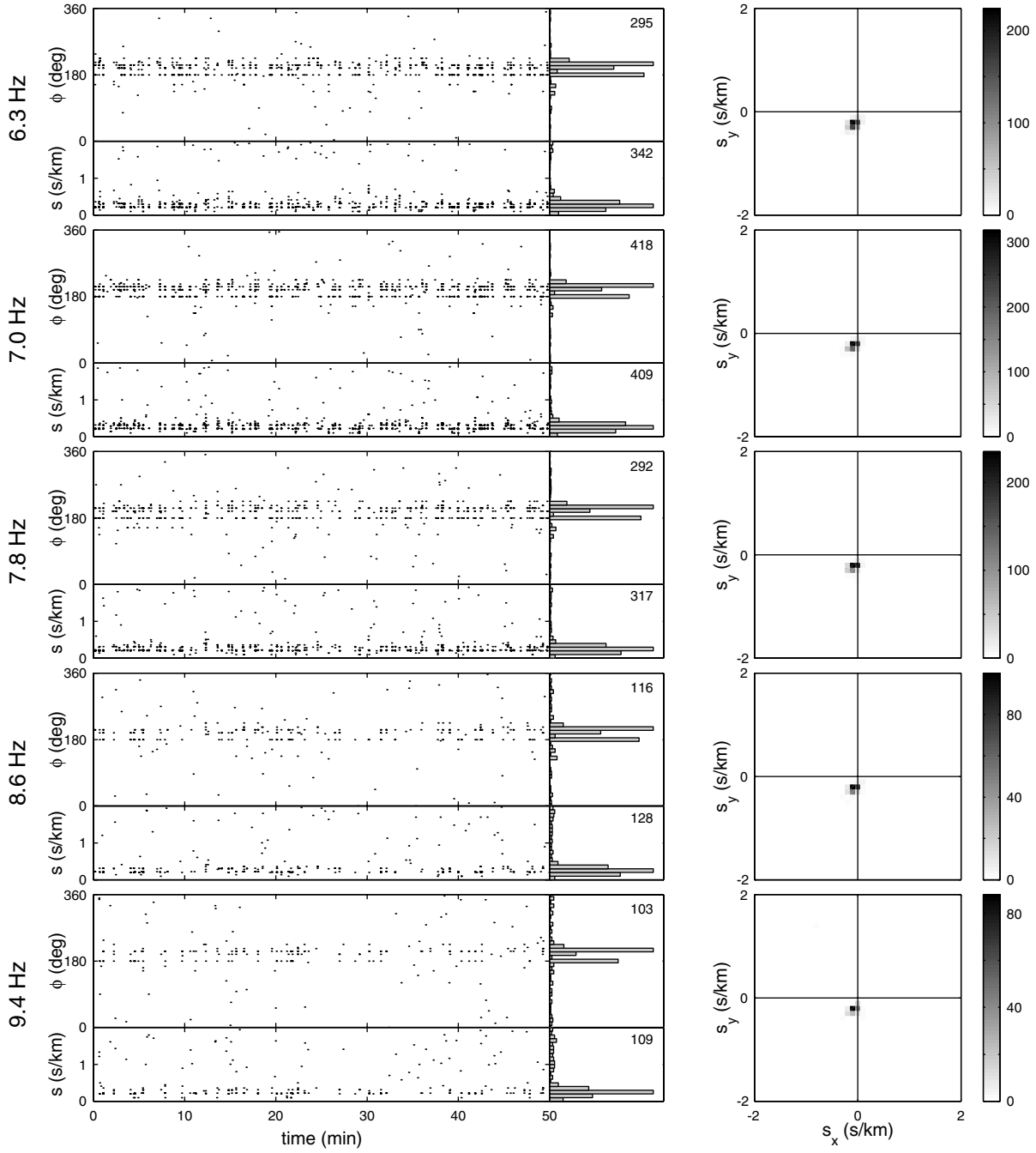

Figure 6. Continued.

activity. We interpret these waves as backscattered waves originating from the scattering of the main component of the wavefield—the background tremor—by topographic features and/or shallow regions with strong velocity contrasts. Because scattering is strongly frequency dependent (e.g., Chernov, 1960; Aki and Chouet, 1975; Wu and Aki, 1985; Chouet, 1990; Sato and Fehler, 1998; Margerin *et al.*, 2000; Lacombe, 2001), this hypothesis is consistent with these waves being only detected in limited frequency bands.

Unlike traditional seismic methods, the use of multiple synchronized antennas allows an estimation of the position of the source of these coherent scattered waves, even if there are no recognizable phases. We use the source location method developed by Almendros *et al.* (2001a) to locate this scattering source. Even though this method was designed to locate LP seismicity, it is independent of the type of signal and can be applied to any signal so long as this signal shows a minimum of coherence that can be recognized simultaneously by multiple antennas. The location procedure consists of a comparison between estimates of the slowness vectors and a slowness vector model calculated at each antenna. Almendros *et al.* (2001a) defined a slowness vector model

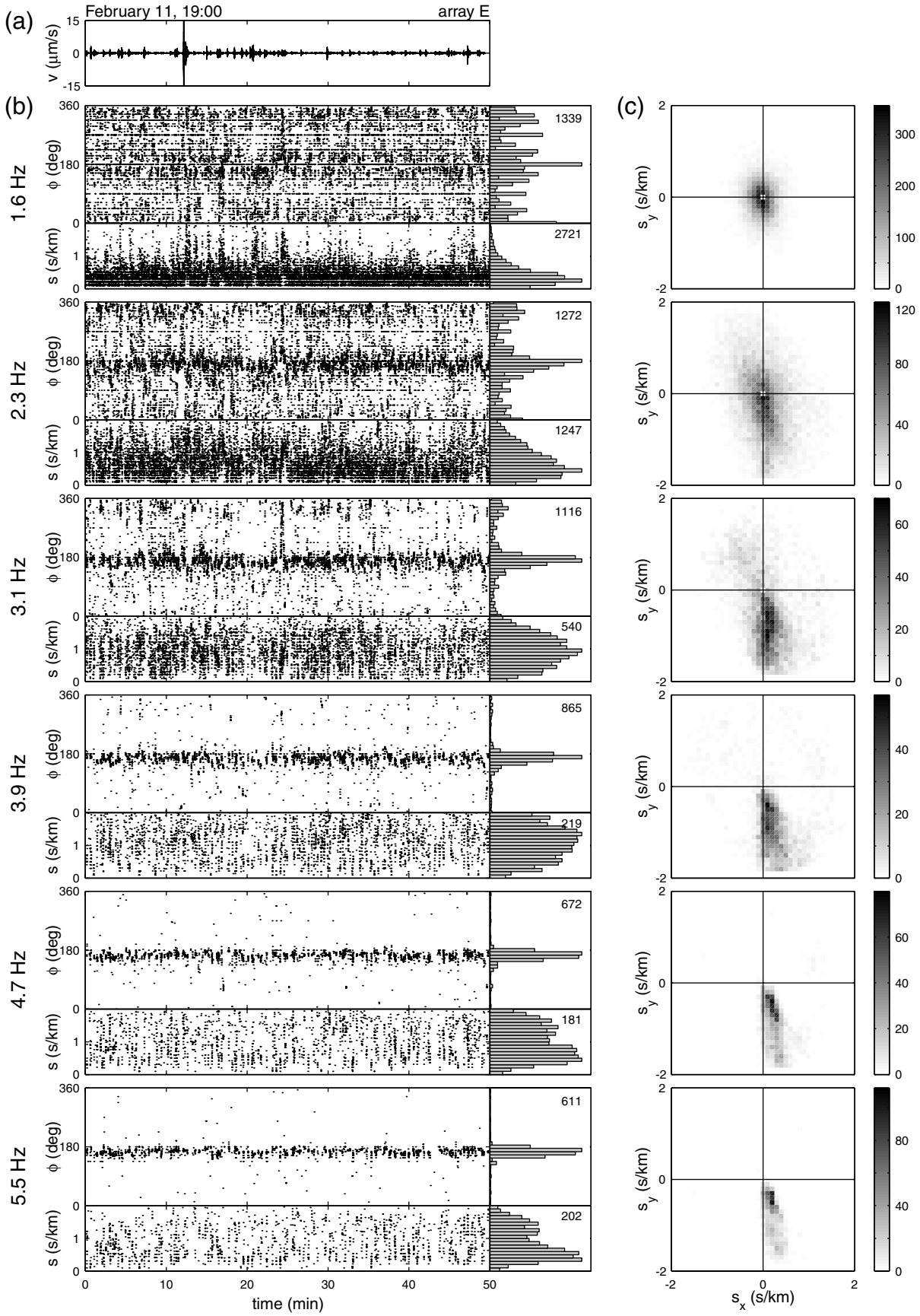

Figure 7. Same as Fig. 6, for antenna E.

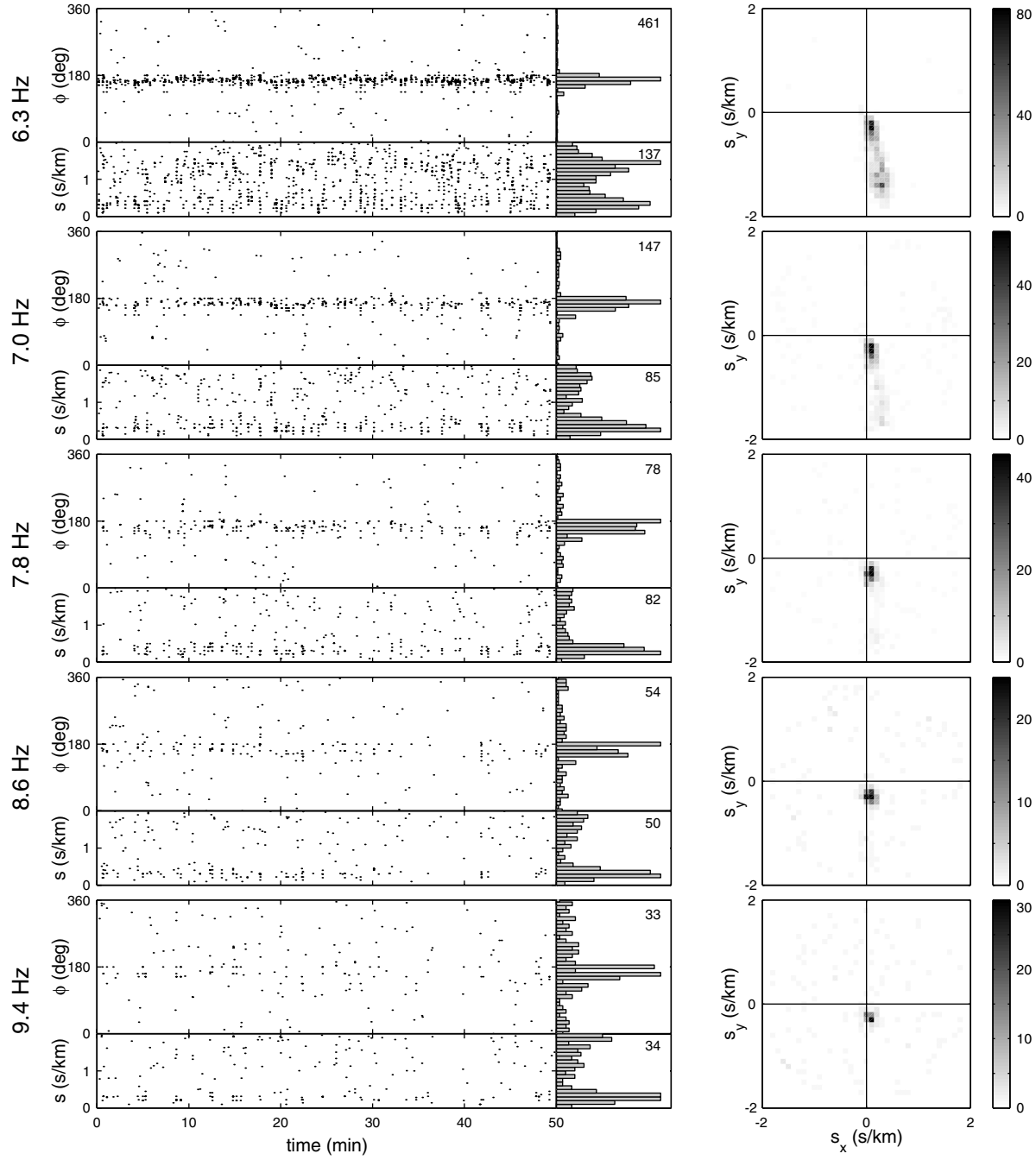

Figure 7. Continued.

for Kilauea volcano based on the topography of Kilauea and the 3D seismic-velocity model of Dawson *et al.* (1999). This slowness model can only account for apparent slownesses ranging up to 0.6 sec/km. The reason for this limitation is the presence of surficial low-velocity layers with combined thicknesses on the order of 100 m and shear wave velocities as low as 300 m/sec (Ferrazzini *et al.*, 1991). Such fine-scale layering is below the resolution of the tomography of Dawson *et al.* (1999). The apparent slownesses ~1.5 sec/km for the scattered wave components observed in our experiment precludes our use of the synthetic slowness vector model of Almendros *et al.* (2001a). Instead, we assume a simplified model consisting of a homogeneous half-space. As we already know that the source is shallow, we only use information about azimuths to obtain an estimate of the epicenter position.

The slowness vectors of the scattered waves are obtained at each antenna as an average of the slowness vector estimates within a time window. The main issue here is to make sure we are detecting simultaneously the same wave fronts at different antennas, because the signal-to-noise ratio is low and no similarities in the waveforms are usually ob-

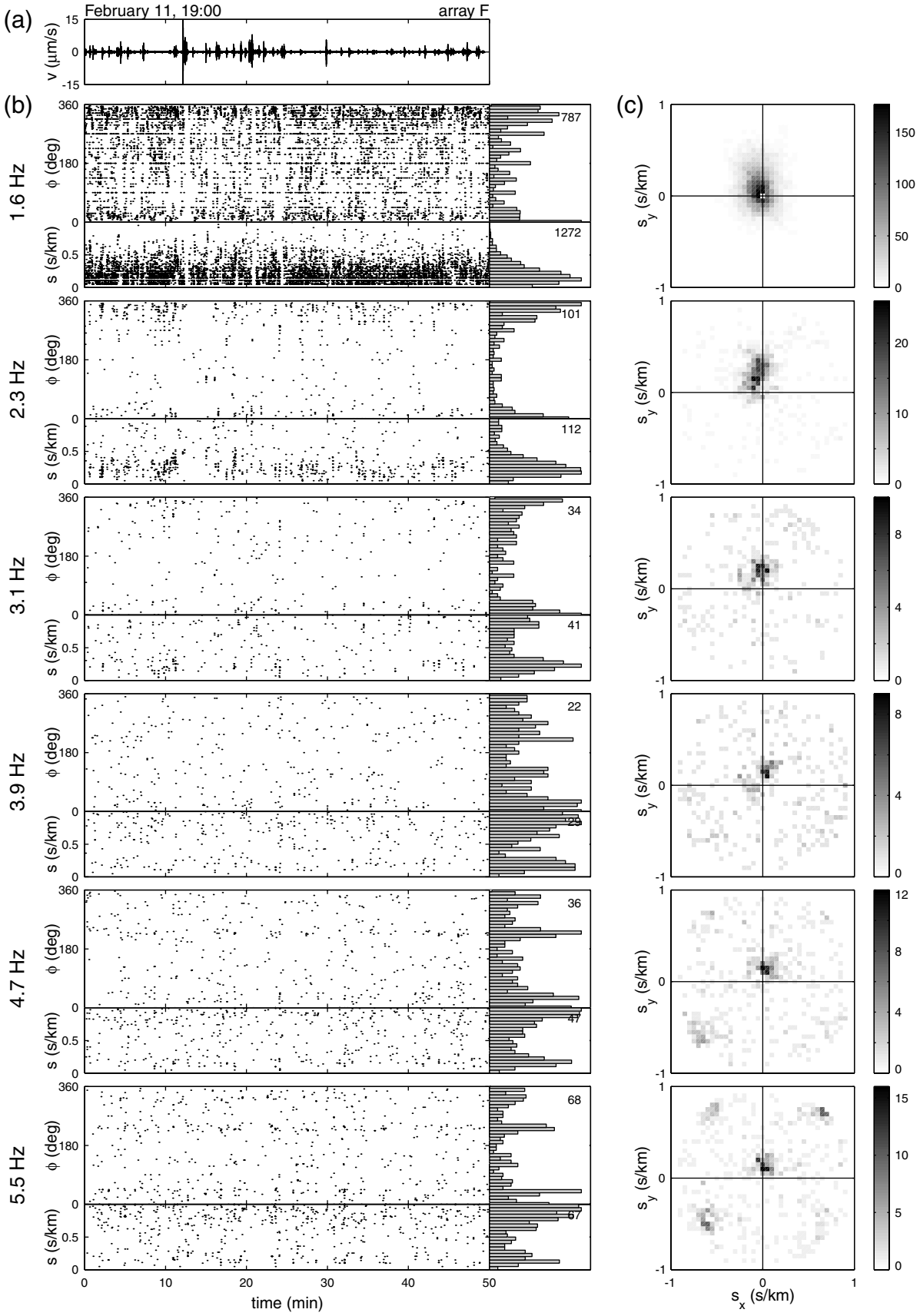

Figure 8. Same as Fig. 6, for antenna F.

Table 1
Most Common Slowness Vectors Observed during the Time Interval Analyzed

Array	Number	Azimuth (°)	Slowness (sec/km)	Frequency Band (Hz)	Period
D	1	210	0.3–0.5	1.6–9.4	1,2
	2	210	~1.5	2.3–5.5	1,2
	3	240	~1.5	3.1–3.9	1
	4	300	~1.5	1.6–3.1	1
	5	—	~0	1.6–2.3	2
E	1	170	0.3–0.5	1.6–9.4	1,2
	2	170	~1.5	2.3–6.3	1,2
	3	330	~1.5	1.6–3.1	1
	4	—	~0	1.6–2.3	2
F	1	355	0.2–0.3	1.6–5.5	1,2
	2	—	~0	1.6–2.3	2

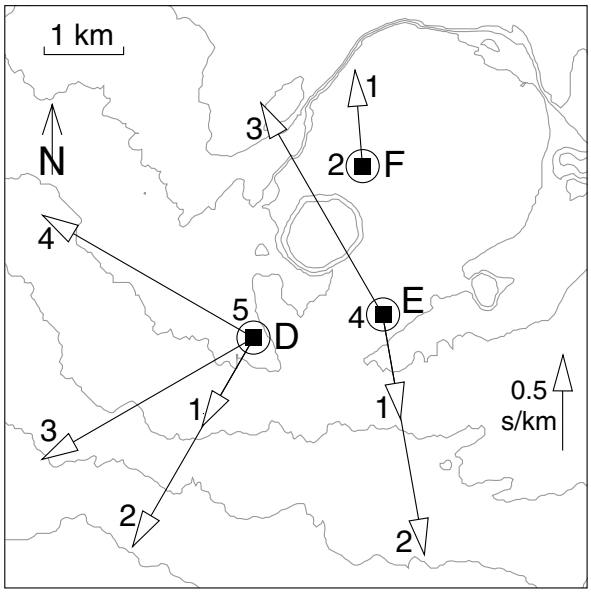

Figure 9. Sketch of the most common slowness vectors observed in the data during the entire time interval analyzed (see Fig. 3–8). The numbers refer to the slowness vectors listed in Table 1. The circles represent slowness vectors with near-zero magnitude.

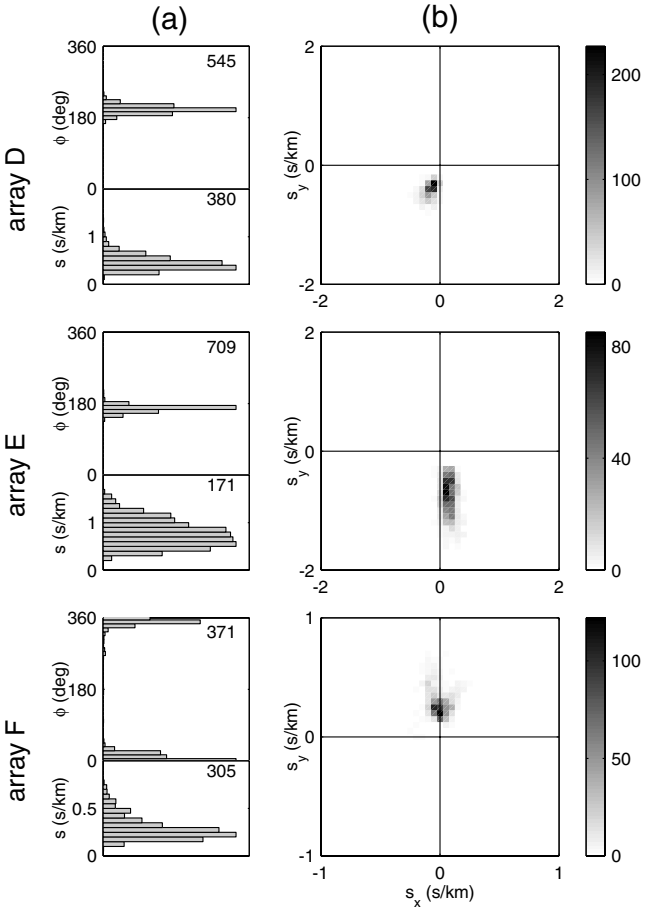

Figure 10. (a) Histograms of azimuths and slownesses and (b) two-dimensional slowness vector histograms for selected LP events and tremor bursts (modified from Almendros *et al.* 2001b).

served. The selection of the windows is based on the presence of stable azimuths corresponding to one of the secondary peaks detected in the azimuth histograms. Our requirement is that this stability be observed simultaneously at antennas D and E within a reasonable delay accounting for the difference in wave propagation times between the two arrays. For the distance of ~1.5 km separating the antennas and observed slownesses near 1.5 sec/km, the maximum expected delay needs to be less 2.5 sec. We selected the frequency band centered at 3.1 Hz, in which the scattered wave fields are most clearly detected (see Figs. 3 and 4). Figure 12 illustrates our window selection procedure. In this example, the predominance of tremor originating from the hydrothermal source near Halemaumau (window A) is interrupted by the arrival of coherent wave fronts with propagation properties corresponding to the slowness vectors D4 and E3 (window B). The common occurrence of vectors D4 and E3 was repeatedly noted throughout period 1. We found 48 time windows in which scattered waves were simultaneously detected at arrays D and E. For each of these windows, a source location was estimated using the method of Almendros *et al.* (2001a). We obtain average values of azimuth and average errors from the frequency–slowness data contained in the selected windows. Then, azimuthal probability functions are defined for each antenna by using the experimental average azimuths as the centers of Gaussian curves with standard deviations of half the average error limits. A spatial probability is assigned to each point in the domain investigated by evaluating the azimuthal probability functions at the azimuth corresponding to the geometric direction from that point to the center of the antennas and multiplying the results obtained from each antenna. We selected a domain of 5 × 5 km, with its northwest corner centered on Halemaumau, and calculated spatial probabilities every 40 m in the north–south and east–west directions.

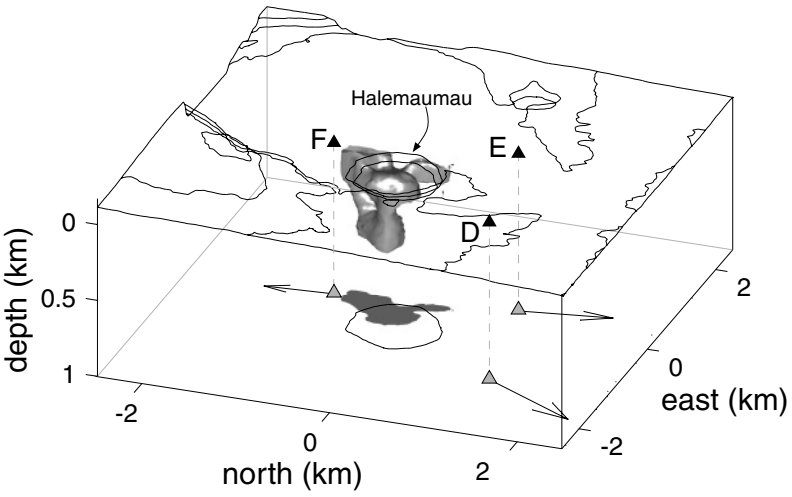

Figure 11. Source location of the main component of the wave field. Solid triangles mark the centers of antennas D, E, and F. The arrows on the bottom plane represent the apparent slowness vectors obtained for the main component of the wave field. Gray triangles in that plane mark the projections of the array positions. The gray region is the LP source region (modified from Almendros *et al.* 2001b), which coincides with the source region of the main component of the wave field. The gray patch overlapping the northeastern edge of Halemaumau (marked by the contour line) is the projection of this region onto the bottom plane.

For each of the 48 selected windows, the maximum of the resulting probability distribution represents the most likely epicenter location. Error limits are defined as the region for which the probability is >80% of the maximum probability. Except for five solutions located on the boundary of the domain, the remainder of locations for the scattering source encompasses a region of ~1 × 1 km centered ~1.5 km south–southeast of antenna E, near the southeast rim of Kilauea caldera (Fig. 13). The position of the scattering source suggests that it may be associated with topographic features, ring fractures, and/or strong lateral velocity contrasts bounding the caldera to the south. Surprisingly, this appears to be the only area along the caldera boundary where energy is efficiently backscattered within the 1–10-Hz band analyzed. A similar observation was reported by Phillips *et al.* (1993), who found scattered phases in the *S*-wave coda of local earthquakes recorded by an array located in the Kanto Basin, Japan. They interpreted the scattering source as a short segment of the basin boundary located closest to the array site. The origin of this effect is not yet clear and will require further study for its elucidation.

Slowness vector D3 may represent a diffraction of the main component of the wave field by the southeastern edge of Halemaumau, which lies between the source and the array. This particular wave-field component is not readily apparent at antenna E. The reason for this may be that Halemaumau does not lie along the direct wave path from the source to array E, so that diffraction effects are minimized at E, or simply that the diffraction component coincides with slowness vector E2, effectively preventing a separation of the two vectors. If the latter is true, one might expect that the two apparent slownesses would be slightly different. This may, in fact, provide an explanation for the extended shape of peak E2, which almost merges with peak E1 (Figs. 4 and 7), in contrast to the two clearly separated peaks D2 and D1 (Fig. 3).

Deep Component

This section focuses on the change in wave-field properties that took place between 02 hr 00 min and 16 hr 00 min on 11 February. After this change, we begin to detect wave-field components D5, E4, and F2, with the following characteristics: (1) these components are mainly detected in the 1.6-Hz band and occasionally in the 2.3-Hz band; (2) the apparent slownesses approach zero, pointing to a quasi-vertical incidence of these waves; (3) as a consequence of the small apparent slownesses, the dispersion in azimuthal values increases, making it difficult to recognize any clustering around specific directions; and (4) these wave-field characteristics remain unchanged through the end of the period analyzed.

The obvious interpretation of these changes is that a deeper source producing coherent energy only in the low-frequency range has become active some time between 02 hr 00 min and 16 hr 00 min on 11 February.

There are several candidate processes that could explain these observations. First is the oceanic microseismic noise. From broadband records, we know that the spectrum of oceanic microtremor is peaked in the frequency range 0.12–0.33 Hz (Dawson *et al.*, 1998), but the spectral cutoff is not very sharp, so that "leakage" of coherent energy in the 1.6- and 2.3-Hz bands is possible. For example, Almendros *et al.* (2000) observed the effect of oceanic noise in their analyses of volcanic earthquakes at Teide volcano, Canary Islands. The wave fields that they sampled contained waves propagating with very low slownesses and quasi-random azimuths in the low-frequency range. However, neither the amplitude nor the character of the oceanic noise observed on the Kilauea broadband seismic network changed during the interval 02 hr 00 min–16 hr 00 min, which casts some doubt about an oceanic origin for the observed signals.

Another explanation may be that we are observing the activation of a deeper magma conduit. Using broadband data recorded at Kilauea caldera, Chouet and Dawson (1997) and Ohminato *et al.* (1998) imaged two colocated seismic sources generating very-long-period (VLP) signals in response to an unsteady flow of magma through a crack-like conduit. The VLP sources are located at a depth of ~1 km below the northeastern edge of Halemaumau. Interestingly,

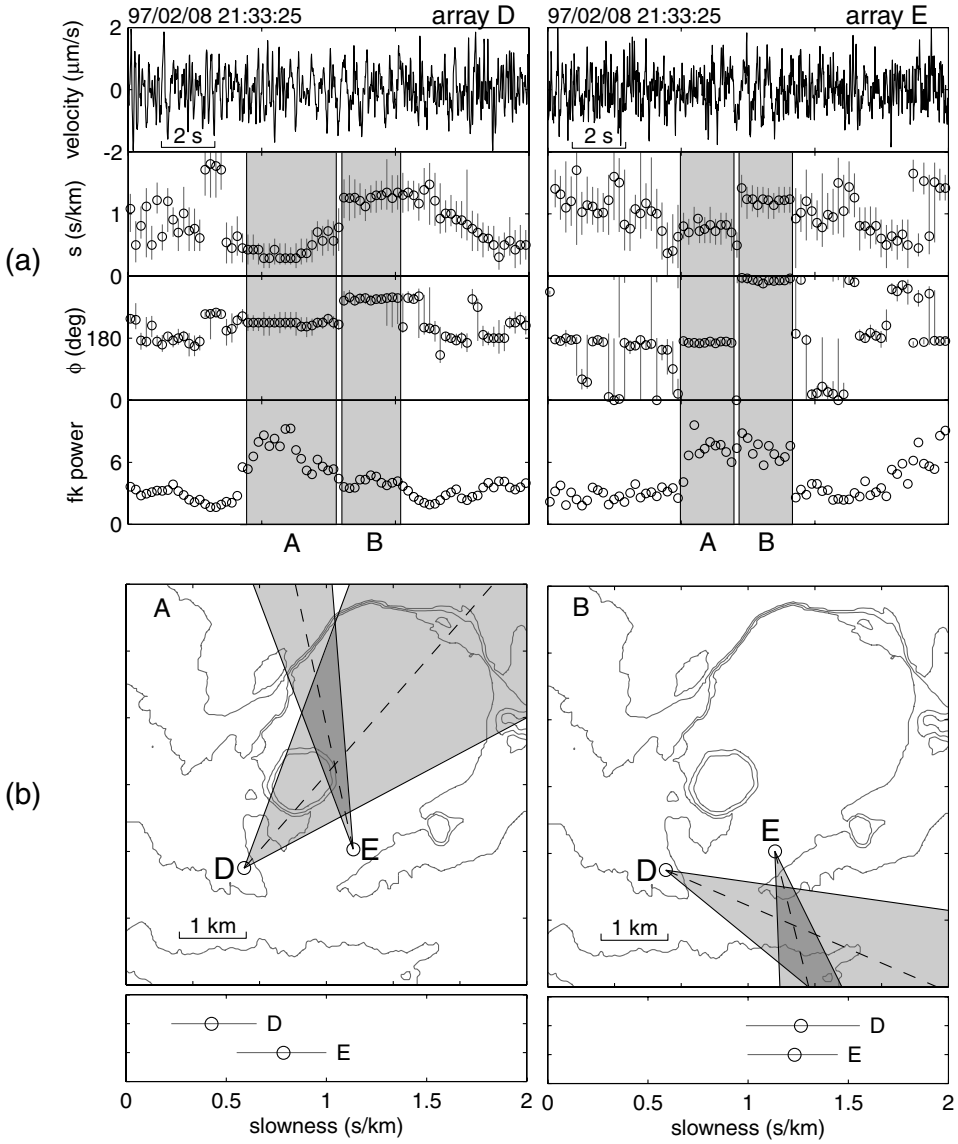

Figure 12. (a) Frequency–slowness results associated with the main peak of the frequency–slowness spectra at 3.1 Hz at arrays D and E. The shaded windows A and B represent intervals during which the same wave-field component propagates simultaneously across the antennas. (b) Epicenter locations and average slownesses obtained during the two time windows shown in (a). The dashed lines represent the average back-azimuths observed during the selected windows, and the shaded azimuthal wedges represent the azimuthal spreads resolved by the antennas. The epicentral region is defined by the overlap of the two azimuthal wedges.

our analysis of broadband records from Kilauea indicates that there was a change in VLP activity at about noon on 11 February, when a series of overlapping pulses with periods of 15 sec was observed to emerge from a quiet VLP background. However, this pulsating activity died out by the morning of 12 February, before the end of the period analyzed, which does not explain why we still detect a deep component of the wave field during the interval from 13 hr 00 min on 12 February through 00 hr 00 min on 13 February. Nevertheless, this hypothesis is particularly interesting because it opens the possibility of finding and documenting a relationship among sources that radiate elastic energy within different frequency bands.

A final possibility is that we are seeing the activation of a deeper part of the Kilauea hydrothermal system. The entire volcanic edifice of Kilauea is permeated by hydrothermal fluids (e.g., Ingebritsen and Scholl, 1993). That only a small region of this hydrothermal system is seismically active during the period we analyze is probably a reflection of a strong upward component in the flow of hot magmatic gases streaming from the magma conduit below Halemaumau. On reaching a certain depth, the gas flux induces pressure per-

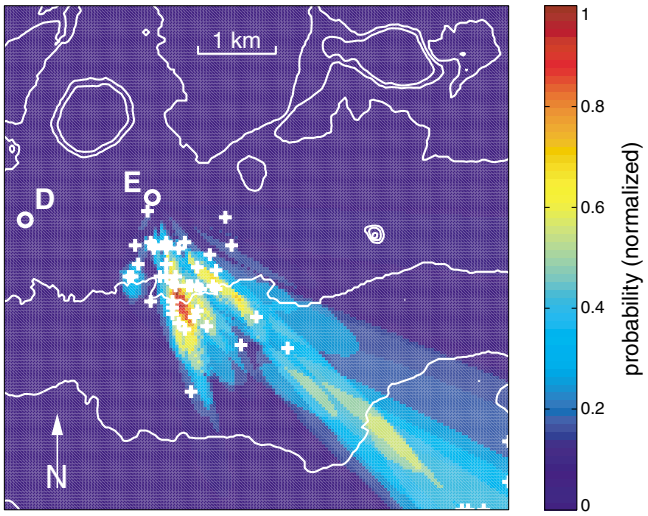

Figure 13. Epicenter locations for 48 samples of backscattered waves. White crosses represent the maxima of the combined spatial probabilities from antennas D and E. Confidence regions are obtained by considering those points where the probability is >80% of the maximum level. The 48 regions are stacked to show the most likely source position (in red).

turbations large enough to generate LP seismicity. This depth is found to be ~500 m for the generation of LP events and ~200 m for tremor (Almendros *et al.*, 2001b), although Almendros *et al.* (2001b) suggest that there may also be deeper sources of tremor that may have been filtered out by their selection of data focused on high-coherence wave packets. Figs. 3–5 demonstrate that background tremor is always present in the wave field. A change in hydrothermal flow conditions could alter those depth limits and produce deeper tremor that could result in the quasi-vertical incidences of the waves detected by the arrays.

Conclusions

The use of multiple, synchronized, seismic antennas constitutes a powerful tool for the analysis of complex wave fields. Each antenna can individually identify different components of the wave field based on the apparent slownesses and azimuths determined from frequency–slowness analyses or a similar method. The combination of several antennas yields an estimate of the location of each component identified simultaneously by at least two antennas and provides a more complete understanding of the wave field.

In the present study, we used three seismic antennas to separate and identify distinct components of the wave fields recorded at Kilauea volcano. We found (1) a sustained background volcanic tremor in the form of body waves generated in the hydrothermal system imaged by Almendros *et al.* (2001b) in their analysis of the LP seismicity; (2) surface waves generated along the path between this hydrothermal source and the antennas; (3) backscattered surface wave energy from a shallow reflector located near the southeastern rim of Kilauea caldera; (4) evidence for diffracted wave components originating at the southeastern edge of Halemaumau; and (5) body waves reflecting the activation of a deeper tremor source between 02 hr 00 min and 16 hr 00 min on 11 February.

We emphasize the importance of two of our results because of their implications for future studies at Kilauea and other volcanoes. First is the detection of a low-amplitude continuous tremor generated in a shallow hydrothermal region northeast of Halemaumau. The presence of this background tremor is hardly noticeable in single-station records. Even though the energy content of the signal is quite weak, the antennas were sensitive enough to detect the radiated wave field and determine its nature and source location. This array-detection capability represents a substantial improvement in the resolution with which we are able to image volcanic processes. Furthermore, the observation of a continuous background tremor originating within the same source as individual LP events supports the idea that LP events are not completely independent events but are part of a sustained activity. As evidenced in our data, tremor can remain sustained over periods of several days. The persistence of tremor requires a physical mechanism of elastic-wave generation that remains continuously active beneath Halemaumau. A possible mechanism that satisfies the observational constraints is the acoustic resonance of fluid-filled cracks triggered by a sustained, unsteady flow of gas through the hydrothermal system (Chouet, 1996). Evidence of such gas flow northeast of Halemaumau comes from carbon dioxide measurements obtained at Kilauea caldera (T. Gerlach, personal comm.). Small bursts in the amplitudes of fluctuating pressure at the source produce slight increases in signal amplitudes, while sharp, short-duration pressure transients at the source lead to the production of LP events (Chouet, 1992, 1996).

Our second significant result is our detection of a source of scattering near the southern rim of Kilauea caldera. Evidence for a scattering source located somewhere south of the antenna E site was documented in an earlier study by Saccorotti *et al.* (2001). Saccorotti *et al.* (2001) only had data from a single antenna and were therefore unable to estimate the distance to the point where the scattered waves were produced. In this sense, we demonstrate that the use of multiple, synchronized, small-aperture antennas represents a step forward in the study of weak, scattered wave components embedded in the wave field. Such analyses yield clues about the spatial distribution of scattering sources and can be useful for mapping heterogeneities in a volcanic edifice.

Acknowledgments

We are grateful to Y. Ida, T. Iwasaki, N. Gyoda, J. Oikawa, M. Ichihara, Y. Goto, T. Kurihara, M. Udagawa, and K. Yamamoto of the Earthquake Research Institute, University of Tokyo; K. Yamaoka, M. Nishihara, and T. Okuda of Nagoya University; H. Shimizu and H. Yakiwara of Kyushu University; E. Fujita of the National Research Institute for Earth Sci-

ence and Disaster Prevention, Tsukuba; T. Ohminato of the Geological Survey of Japan, Tsukuba; S. Adachi of Hakusan Corporation; C. Dietel and P. Chouet of the U.S. Geological Survey, Menlo Park; P. Okubo, A. Okamura, M. Lisowski, M. Sako, K. Honma, and W. Tanigawa of the U.S. Geological Survey, Hawaiian Volcano Observatory; S. McNutt, D. Christensen, and J. Benoit of the University of Alaska, Fairbanks; and S. Kedar of the California Institute of Technology, Pasadena, for their participation in the field experiment. In particular, we wish to thank Y. Ida, whose exceptional organizational skills made this experiment possible. Funding for the experiment was provided by a grant from the Japanese Ministry of Education (Monbusho) to the Earthquake Research Institute of the University of Tokyo. Arthur McGarr and David Hill contributed with constructive comments. The work by J. Almendros was supported by a fellowship from the Spanish Ministry of Education and by projects REN-2001-3833 and REN-2001-2814-C04-04 of the Spanish Ministry of Science and Technology.

References

Aki, K. (1957). Space and time spectra of stationary stochastic waves, with special reference to microtremors, *Bull. Earthquake Res. Inst. Tokyo Univ.* **25,** 415–457.

Aki, K., and B. Chouet (1975). Origin of coda waves: source, attenuation and scattering effects, *J. Geophys. Res.* **80,** 3322–3342.

Almendros, J., B. Chouet, and P. Dawson (2001a). Spatial extent of a hydrothermal system at Kilauea Volcano, Hawaii, determined from array analyses of shallow long-period seismicity, part I: method, *J. Geophys. Res.* **106,** 13,565–13,580.

Almendros, J., B. Chouet, and P. Dawson (2001b). Spatial extent of a hydrothermal system at Kilauea Volcano, Hawaii, determined from array analyses of shallow long-period seismicity, part II: results, *J. Geophys. Res.* **106,** 13,581–13,597.

Almendros, J., B. Chouet, and P. Dawson (2002). Array detection of a moving source, *Seism. Res. Lett.* **73,** 153–165.

Almendros, J., J. Ibáñez, G. Alguacil, and E. Del Pezzo (1999). Array analysis using circular wavefront geometry: an application to locate the nearby seismo-volcanic source, *Geophys. J. Int.* **136,** 159–170.

Almendros, J., J. M. Ibáñez, E. Del Pezzo, R. Ortiz, G. Alguacil, M. La Rocca, M. J. Blanco, and J. Morales (2000). A seismic antenna survey at Teide Volcano: evidences of local seismicity and inferences from non-existence of volcanic tremor, *J. Volcan. Geotherm. Res.* **103,** 439–462.

Capon, J. (1969). High-resolution frequency-wavenumber spectrum analysis, *Proc. IEEE* **57,** 1408–1418.

Chernov, L. A. (1960). *Wave Propagation in a Random Medium*, McGraw-Hill, New York.

Chouet, B. (1990). Effect of anelastic and scattering structures of the lithosphere on the shape of local earthquake coda, *PAGEOPH* **132,** 289–310.

Chouet, B. (1992). A seismic model for the source of long-period events and harmonic tremor, in *IAVCEI Proceedings in Volcanology, Vol. 3*, Johnson, R. W., G. Mahood, and R Scarpa (editors), Springer-Verlag, Berlin, 133–156.

Chouet, B. (1996). Long-period volcano seismicity: its source and use in eruption forecasting, *Nature* **380,** 309–316.

Chouet, B. A., and P. B. Dawson (1997). Observations of very-long-period impulsive signals accompaying summit inflation at Kilauea volcano, Hawaii, in February 1997, (abstract), *EOS Trans. AGU* fall meeting supplement, **76,** S11C-3.

Chouet, B., G. De Luca, G. Milana, P. Dawson, M. Martini, and R. Scarpa (1998). Shallow velocity structure of Stromboli volcano, Italy, derived from small-aperture array measurements of strombolian tremor, *Bull. Seism. Soc. Am.* **88,** 653–666.

Chouet, B., G. Saccorotti, M. Martini, P. Dawson, G. De Luca, G. Milana, and R. Scarpa (1997). Source and path effects in the wavefields of tremor and explosions at Stromboli volcano, Italy, *J. Geophys. Res.* **102,** 15,129–15,150.

Dawson, P., B. Chouet, P. Okubo, A. Villaseñor, and H. Benz (1999). Three-dimensional velocity structure of the Kilauea caldera, Hawaii, *Geophys. Res. Lett.* **26,** 2805–2808.

Dawson, P., C. Dietel, B. Chouet, K. Honma, T. Ohminato, and A. Okubo (1998). Digitally telemetered broadband seismic network at Kilauea Volcano, Hawaii, *U.S. Geol. Surv. Open-File Rep.* **98–108,** 122 p.

De Luca, G., R. Scarpa, E. Del Pezzo, and M. Simini (1997). Shallow structure of Mt. Vesuvius volcano, Italy, from seismic array analysis, *Geophys. Res. Lett.* **24,** 481–484.

Del Pezzo, E., J. Ibáñez, and M. La Rocca (1997). Observations of high-frequency scattered waves using dense arrays at Teide volcano, *Bull. Seism. Soc. Am.* **87,** 1637–1647.

Ferrazzini, V., K. Aki, and B. Chouet (1991). Characteristics of seismic waves composing hawaiian volcanic tremor and gas-piston events observed by a near-source array, *J. Geophys. Res.* **96,** 6199–6209.

Goldstein, P., and R. Archuleta (1989). Array analysis of seismic signals, *Geophys. Res. Lett.* **14,** 13–16.

Goldstein, P., and B. Chouet (1994). Array measurements and modeling of sources of shallow volcanic tremor at Kilauea volcano, Hawaii, *J. Geophys. Res.* **99,** 2637–2652.

Gupta, I. N., C. S. Lynnes, T. W. McElfresh, and R. A. Wagner (1990). F-k analysis of NORESS array and single station data to identify sources of near-receiver and near-source scattering, *Bull. Seism. Soc. Am.* **80,** 2227–2241.

Ibáñez, J. M., J. Almendros, G. Alguacil, E. Del Pezzo, M. La Rocca, R. Ortiz, and A. García (2000). Seismo-volcanic signals at Deception Island volcano (Antarctica): wavefield analysis and source modeling, *J. Geophys. Res.* **105,** 13,905–13,931.

Ingebritsen, S. E., and M. A. Scholl (1993). The hydrogeology of Kilauea Volcano, *Geothermics* **22,** 255–270.

Lacombe, C. (2001). Propagation des ondes élastiques dans la lithosphère hétérogène: modélisations et applications, *Ph.D. Thesis*, University of Grenoble, Grenoble, France, 162 p.

LaCoss, R. T., E. J. Kelly, and M. N. Toksöz (1969). Estimation of seismic noise structure using arrays, *Geophysics* **34,** 21–38.

Margerin, L., M. Campillo, and B. Van Tiggelen (2000). Monte Carlo simulation of multiple scattering of elastic waves, *J. Geophys. Res.* **105,** 7873–7892.

Métaxian, J. P., P. Lesage, and J. Dorel (1997). Permanent tremor of Masaya volcano, Nicaragua: wavefield analysis and source location, *J. Geophys. Res.* **102,** 22,529–22,545.

Ohminato, T., B. Chouet, P. Dawson, and S. Kedar (1998). Waveform inversion of very long period impulsive signals associated with magmatic injection beneath Kilauea volcano, Hawaii, *J. Geophys. Res.* **103,** 23,839–23,862.

Phillips, W. S., S. Kinoshita, and H. Fujiwara (1993). Basin-induced Love waves observed using the strong-motion array at Fuchu, Japan, *Bull. Seism. Soc. Am.* **83,** 64–84.

Sato, H., and M. Fehler (1998). *Seismic Wave Propagation and Scattering in the Heterogeneous Earth*, Springer-Verlag, New York.

Saccorotti, G., B. Chouet, and P. Dawson (2001). Wavefield properties of a shallow long-period event and tremor at Kilauea volcano, Hawaii, *J. Volcan. Geotherm. Res.* **109,** 163–189.

Schmidt, R. O. (1986). Multiple emitter location and signal parameter estimation, *IEEE Trans. Ant. Prop.* **34,** 276–280.

Wu, R. S., and K. Aki (1985). Elastic wave scattering by a random medium and the small-scale inhomogeneities in the lithosphere, *J. Geophys. Res.* **90,** 10,261–10,273.

U.S. Geological Survey
Menlo Park, California
(J.A., B.C., P.D.)

University of Geneva
Geneva, Switzerland
(C.H.)

Manuscript received 24 January 2002.